[1]Laboratory of Cloud-Precipitation Physics and Severe Storms
Institute of Atmospheric Physics
Chinese Academy of Sciences, Beijing 100029, China

[2]Shandong Provincial Meteorological Center, Jinan, Shandong 250031, China

[3]School of Meteorology and [4]Center for Analysis and Prediction of Storms
University of Oklahoma, Norman, Oklahoma 73019, USA

Short-range Prediction of a Heavy Precipitation Event by Assimilating Chinese CINRAD-SA Radar Reflectivity Data using Complex Cloud Analysis

Chunyan Sheng [1,2], Shouting Gao[1] and Ming Xue[3,4]

With 13 Figures

Submitted to Meteorol. Atmos. Phys.

May 2005

Corresponding author address:
Dr. Chunyan Sheng
Laboratory of Cloud-Precipitation Physics and Severe Storms (LACS)
Institute of Atmospheric Physics
Chinese Academy of Sciences
Beijing 100029, China

E-mail: scy9186@yahoo.com.cn

Summary

With the ARPS (Advanced Regional Prediction System) Data Analysis System (ADAS) and its complex cloud analysis scheme, the reflectivity data from a Chinese CINRAD-SA Doppler radar are used to analyze 3D cloud and hydrometeor fields and in-cloud temperature and moisture. Forecast experiments starting from such initial conditions are performed for a northern China heavy rainfall event to examine the impact of the reflectivity data and other conventional observations on short-range precipitation forecast.

The full 3D cloud analysis mitigates the commonly known spin-up problem with precipitation forecast, resulting a significant improvement in precipitation forecast in the first 4 to 5 hours. In such a case, the position, timing and amount of precipitation are all accurately predicted. When the cloud analysis is used without in-cloud temperature adjustment, only the forecast of light precipitation within the first hour is improved.

Additional analysis of surface and upper-air observations on the native ARPS grid, using the 1 degree real-time NCEP AVN analysis as the background, helps improve the location and intensity of rainfall forecasting slightly. Hourly accumulated rainfall estimated from radar reflectivity data is found to be less accurate than the model predicted precipitation when full cloud analysis is used.

1. Introduction

Accurate quantitative precipitation forecasting (QPF) is one of the most challenging tasks of numerical weather prediction (NWP), especially in the first few hours of forecast. The main sources of the difficulties in the initial hours lie with the deficiencies in the initiation-condition definition of moisture, cloud and hydrometeor fields, and the latent heating and circulations associated with ongoing precipitation. Such deficiencies create the commonly known model "spin-up" problem (e.g., Kasahara et al. 1988) which under-predicts rainfall in at least the first few hours. In order to reduce the needed "spin-up" time and improve short-term QPF, various techniques of diabatic initialization and data assimilation have been developed in the recent years. For example, rainfall observations have been used to correct humidity and/or temperature profiles in the initial conditions in order to obtain precipitation prediction that is closer to measurements (Krishnamurti et al. 1993; Wu et al. 1995). Methods employing nudging for rainfall assimilation have attained positive impact on both precipitation forecast and the model dynamical fields in several studies (Manobianco et al. 1994; Falkovich et al. 2000; Davolio and Buzzi 2004). In recent years, satellite data have also been used to improve the initial model fields and to mitigate the "spin-up" problem (e.g., Puri and Miller 1990; Puri and Davidson 1992; Weng and Liu 2003; Lee and Lee 2003; Yucel et al. 2003). Other works make use of radar data, to estimate precipitation rate and the latent heating profile and to apply the latent heating effect and/or moisture adjustments to the model fields (e.g., Wang and Warner 1988; Takano and Segami 1993; Aonashi 1993). In Rogers et al. (2000), the radar data are used indirectly, for determining when and where deep moist convection is occurring, and the information is used to activate the convective parameterization scheme of the prediction model at the right locations. All of these studies have demonstrated positive impact of assimilating precipitation information

observed by satellite, radar and/or surface stations, on reducing the spinup problem and in improving precipitation forecast. Most of these studies do not, however, use the radar reflectivity observations to directly specify or analyze the moisture, temperature and/or cloud microphysical fields that are related to precipitation systems.

Since the deployment of the Next Generation WSR-88D Doppler radar network in the US in the 1990s, an increasing amount of efforts has been placed upon the use of Doppler radar data for storm-scale numerical model initialization and forecast because of the high spatial and temporal resolutions of such data. In recent years, a three-dimensional (3D) cloud analysis system that uses radar reflectivity, along with satellite and surface observations of clouds, has been developed at the Center for Analysis and Prediction of Storms (CAPS) of the University of Oklahoma (Zhang et al. 1998; Zhang 1999; Brewster 2002). Combining 3D volume scans of radar reflectivity, surface cloud observations and satellite infrared and visible imagery data, with a high-resolution background analysis that has already incorporated conventional observations as well as Doppler radar radial velocity data, the 3D fields of cloud and hydrometeors, as well as the water vapor and temperature perturbations due to the cloud and precipitation, are determined. Case studies have been performed using the cloud analysis within the framework of the Advanced Regional Prediction System (ARPS) and its data assimilation system, and the results generally show positive impact on convective storm initialization and precipitation forecast, although the degree of impact depends on the type of storms, and if the systems are strongly forced.

Hu et al. (2005a,b) applied the ARPS cloud analysis scheme together with the ARPS 3DVAR (Gao et al. 2004) to a weakly forced tornadic thunderstorm case, and found that the use of the full cloud analysis within intermittent assimilation cycles was critical. Without the cloud

analysis, the model failed to initialize and predict most of the observed thunderstorms. With the full assimilation procedure, a cluster of supercell storms was accurately analyzed and predicted, for up to two hours. The rotating characteristics of the supercell storm that spawned two tornadoes were well captured, with forecast timing errors being less than 15 minutes and location errors less than 10 km at the times of tornado occurrence during the second hour. With their 3DVAR and cloud analysis procedure, reflectivity data were found to have more positive impact than radial velocity. In Dawson and Xue (2005), the ARPS cloud analysis procedure was shown to help reduce the spin up time of an organized mesoscale convective system (MCS) by about two hours. Due to the presence of strong synoptic scale forcing, the MCS was able to develop even without cloud analysis, but the initiation was delayed by about two hours, which resulted in significant position errors of the propagating MCS in the subsequent 6-8 hours of forecast. Both studies used full-volume data from the US WSR-88D radars.

A much simplified version of the ARPS cloud analysis, which builds cloud fields and adjusts the moisture based on the NCEP AVN forecast, was applied to the generally rainy and mountainous region of northwestern Spain by Souto et al. (2003), and positive effects were also found on precipitation forecast via month-long verification scores.

In this study, we apply the ARPS Data Analysis System (ADAS) and its cloud analysis procedure to a northern China region, using data from a Chinese CINRAD-SA Doppler radar. The SA Doppler radar, also called WSR-98D, is part of the Chinese new generation weather radar network. It is an S-band radar whose characteristics are similar to those of the WSR-88D radars in the US operational Doppler radar network (Zhu and Zhu 2004). The impact of reflectivity on QPF is examined for a heavy rainfall event, through sensitivity experiments with/without cloud analysis and the associated temperature adjustment. We consider the

application to a new geographic region and to a different type of precipitation system, using data from a different radar system, the new aspects of this study.

The rest of this paper is organized as follows. In section 2, the ARPS model and its data analysis system ADAS are briefly described. In section 3, an overview of the heavy rainfall event and the design of the numerical experiments are introduced. In section 4, the results of four experiments are discussed in detail. Section 5 contains a comparison between radar-based hourly accumulated precipitation estimates and the model predicted rainfall. Summary and conclusions are given in section 6.

2. ARPS and ARPS Data Analysis System (ADAS)

The numerical model used in this study is the Advanced Regional Prediction System (ARPS, Xue et al. 1995; 2000; 2001; 2003) developed at the Center for Analysis and Prediction of Storms (CAPS), the University of Oklahoma. It is a multi-scale compressible nonhydrostatic prediction system that includes data ingest, quality control, data analysis and assimilation procedures, the prediction model, and post-processing packages. It has been used for the simulation and prediction of a wide range of atmospheric phenomena.

The ARPS Data Analysis System (ADAS, Brewster 1996) is based on the Bratseth (1986) successive correction method, which can converge to the optimal interpolation (OI) solution. The basic analysis variables of the ADAS are the same as, or can be converted easily to, the model prognostic variables, such as temperature, pressure, humidity, and the velocity components. As mentioned earlier, the ADAS includes a complex cloud analysis component which is capable of ingesting Doppler radar, satellite, and surface cloud observations for performing a 3D cloud analysis that adjusts the cloud and hydrometeor contents and the humidity and temperature fields. Details on the package can be found in Zhang et al. (1998) and Zhang (1999) while more

recent improvements are described in Brewster (2002) and Hu et al. (2005a). In this study, we use the temperature adjustment procedure documented in Zhang (1999), that is based on the latent heat release associated with observed reflectivity.

3. The 10-12 October 2003 north China heavy rainfall event and experimental design

a. The 10-12 October 2003 heavy rainfall event

A heavy rainfall event occurred on 10-12 October 2003, caused mainly by a cold front intruding into a warm inverted trough at the surface (Fig. 1a) and by a shear line with an embedded mesoscale vortex in the lower troposphere (Fig. 1b). The maximum total rainfall of this event was around 254 mm, measured by a rain gauge in Ningjin county, Dezhou city in the northwest part of Shandong province (SD, as marked in Fig. 3). It was the highest single-event rainfall amount of this season during the recent 50 years of history in this region. In the morning of 11 October 2003 (LST), the surface cold front arrived at the west part of SD, and associated with it was a band of severe precipitation along the lower reach of the Yellow (Huanghe) River or the stretch of the river within SD. The 850hPa chart (Fig. 1b) shows a newly formed mesoscale vortex on a shear line that intensified over the next 12 hours. The maximum 6-hour precipitation was at least 79 mm in the northwest part of SD. At that time, the Yellow River was at the verge of overflow because of continual heavy precipitation of previous days in the upper and middle reaches of the river. Given such a circumstance, precise forecasting of rainfall amount and location was extremely important for the region. Most real-time NWP forecasts did not provide accurate location forecast of the precipitation in SD; they also under-predicted the amount. As a result, over ten cities in SD suffered from severe flooding, and the coastal regions also suffered from storm tides. The disaster in Heze City in the southwest of SD near the Yellow River was most severe, because of being located within the river flood plain. This heavy rainfall

event was within the observing range of the CINRAD-SA Doppler radar located in Qihe county at 36.8°N, 116.8°E (marked by the black dot in Fig. 3). The composite reflectivity image from Qihe radar at 00 UTC 11 Oct. 2003 is shown in Fig.2. With a particular emphasis on QPF, this study examines for this case the effect of radar data assimilation in a mesoscale model.

b. Experimental design

All experiments use two-level one-way nested grids. Their horizontal resolutions are 30 and 6 km, and cover squared domains of 3000 and 900 km wide, respectively (see Fig. 3). In the vertical, these two domains consist of 43 and 53 sigma-z levels, respectively, both with a minimum thickness layer of about 20 m near the surface and vertically stretched grids extending to model tops at about 20 km height. The two domains are centered at 36°N, 116°E and 36.8°N, 116.8°E, respectively. In all experiments, the full physics mode of ARPS is used, including a two-layer soil-vegetation model, Lin et al (1983) ice microphysics, TKE-based subgrid-scale turbulence and PBL parameterizations, and full long- and short-wave radiation. The Kain-Fritsch convective parameterization scheme is used only on the 30 km domain. The terrain definitions are created from a 30-second global terrain data base, for the two domains separately, and the 6-km terrain transitions gradually towards that of coarse grid in a boundary zone of several grid point wide.

A single 30-km model forecast is made, starting from the 1-degree NCEP real-time global AVN analysis at 00 UTC 11 October 2003, and using 6-hourly analyses from the same data set for lateral boundary conditions. Figure 4a shows the 30-km resolution model-predicted pressure and the wind field at 850hPa at 06 UTC, as compared to those of NCEP analysis in Fig. 4b. It is clear that the lower tropospheric flow pattern, including the southwest-northeast oriented shear line and the embedded vortex, is well reproduced by the model. The vortex center is located over

southwestern SD. Near the southeast corner of the plotted domain is a tropical low pressure system and a narrow high-pressure ridge in between. These systems help keep the mid-latitude systems in place hence prolong the precipitation. The vortex and shear line maintains their 00 UTC 11 locations for nearly 12 hours and then starts to move slowly eastwards.

Four 6-km experiments are performed (see Table 1). They are designed to examine the impact of radar reflectivity data via cloud analysis on QPF. The 6-km grid uses 3-hourly forecasts from the 30 km grid for boundary conditions (tests with hourly boundary conditions did not show much difference). All simulations are initialized at 00 UTC 11 October 2003 and run for 6 hours, to 06 UTC of the same day. For the control experiment, known as CNTL, additional analysis is performed on the 6-km grid, using conventional surface and sounding observations, with the AVN analysis used as the background. Reflectivity data are not used therefore cloud analysis is not performed for CNTL.

Experiment CLD performs the cloud analysis at the initial time, 00 UTC, but without adjustment to the in-cloud temperature that is part of the standard ADAS cloud analysis scheme while in experiment CLDT, this temperature adjustment is activated. The temperature adjustment accounts for latent heating effect from existing clouds and precipitation and generally helps sustain convection. The last experiment, CLDTNCO, is similar to CLDT but excludes all conventional observations in the ADAS analysis; in another word, cloud analysis is directly performed over the NCEP AVN analysis background. The cloud analysis uses Level-II reflectivity data from the Chinese CINRAD Doppler radar at Qihe site. The data include 9 tilts and the scans are in precipitation mode. In all experiments including the cloud analysis, microphysical fields are adjusted based on the reflectivity formula of Smith et al. (1975). Comparisons with alternative formula are made in Hu et al (2005a), and the currently used

version is recommended. The results of the four 6-km experiments are the primary focus of this study.

4. Results of 6-km experiments

a. Initialization of cloud microphysical fields and temperature perturbations

In the initial condition of CNTL, the mixing ratios of rain water (q_r), cloud ice (q_i), snow (q_s) and hail (q_h) are zero everywhere, although the AVN analysis does carry variable q_c, the liquid cloud water mixing ratio. After the complex cloud analysis using radar reflectivity data, q_c, q_r, q_i, and q_s are all adjusted within the radar observation range. Along 37°N, an east-west vertical cross-section of the increments of initial q_c, q_r, q_i, and q_s in the experiments with cloud analysis is shown in Fig.5. As seen in Fig.5a, q_c is significantly enhanced below the 6-km level within the radar coverage, with three regions of high values in this cross-section. A maximum exceeding 1.2 g kg^{-1} is found at 117°E at about 4 km level. The regions of high q_c correspond well with radar echo pattern shown in a cross-section along the same latitude (Fig. 6**)**. The rainwater mixing ratio q_r is mainly found below 5 km level, where temperature is above 0°C (Fig. 5b). The q_i (Fig.5c) and q_s (Fig.5d) added by the cloud analysis are somewhat similar in distribution although q_s extends a higher level, with the 0.05 g kg^{-1} contour reaching 11 km. The adjustment to the potential temperature (θ) is given in Fig.5e, and its pattern is similar to q_c because it is adjusted based on the latent release of cloud water and ice. The maximum θ increment exceeds 4 K at about 117°E and 5 km height.

b. Comparisons of 6-h accumulated precipitation

Figures 7a through 7d show the 6-h accumulated forecast rainfall from the four 6-km experiments, respectively. At a glance, the predicted rainfall distributions of the four are similar:

they all show a band of heavy precipitation extending from northeast to the southwest into the northwestern part of Shandong Province. The precipitation region then further extends southwards through central Shandong into Anhui and Jiangsu provinces located immediately south. All experiments show three general areas of high precipitation, with the strongest one being located at the extreme north of Shandong, a weaker one in the south part of the province and the third one close to the southern boundary the plotted domain. The actual amount and location of these high precipitation centers are, however, quite different across the experiments.

The precipitation is the lightest in CNTL, as shown in Fig.7a. The amount corresponding to the overall maximum center is about 70 mm versus the observed 79 mm (Fig. 7e), which is not bad. In comparison with rain gauge observations, the rainfall is generally under-predicted along the main precipitation band, and more so over the southern portion of the band. In fact, where the second maximum center of 50 mm is found (Fig. 7e), the model predicted precipitation is less than 10 mm (Fig. 7a). It does predict, as the other three experiments also do, a southward stretch of precipitation band of over 30 mm, which roughly matches the observed southward extension of between 20 and 30 mm (Fig. 7e).

The general distribution of rainfall from experiment CLD, which used cloud analysis without temperature adjustment, is similar to that of CNTL but the maximum amount is increased to 80 mm (Fig. 7b), much closer to the observed 79 mm. Experiment CLD, however, still suffers from not being able to produce enough precipitation along the southern portion of the main precipitation band.

The forecast rainfall of CLDT, which adds on top of CLD temperature adjustment, shows an improved pattern along the main precipitation band (Fig. 7c); over 30 mm of precipitation is now predicted close to the center of 50 mm observed rainfall, and as a result, the precipitation

exhibits a more northeast-southwest orientation that is closer to the observation. The overall maximum is, however, increased to 90 mm, above the observed 79 mm. Such a difference, similar in absolute value to that of CNTL, is believed to be within the range of rainfall observation representativeness errors. In addition, the rainfall in south SD is decreased slightly, to values that are closer to observations, but this improvement may or may not be significant.

The rainfall pattern predicted by CLDTNCO, the experiment with full cloud analysis but without conventional observations, is similar to that of CLDT but the maximum rainfall is over 110 mm, about 30 mm above the observed value. Assuming the rain gauge observations are reasonably accurate, in their spatial presentation, this experiment suggests that the analysis of convectional surface and upper-air observations by ADAS, directly on the 6-km ARPS grid, adds value to the coarse resolution AVN analysis. Some reasons for the differences between CLDT and CLDTNCO will be discussed in the next subsection.

Evidently, the cloud analysis, especially when including the temperature adjustment, improves the 6-h accumulated precipitation forecast, in both amount and spatial distribution. The 're-analysis' of convectional data, on the native model grid, is also beneficial. On the other hand, the experiment without cloud analysis is able to predict the center of maximum 6-h precipitation almost equally well, suggesting that at least in this particular area, the convection is strong forced. Indeed, the intense lower mid-tropospheric mesoscale vortex and the shear line discussed earlier provide such a forcing. In the next subsection, we will compare precipitation forecasts at hourly intervals.

c. Hourly precipitation forecasts

To assess both the spatial and temporal accuracies of the QPF, especially during the earlier hours when the spinup problem usually exists without diabatic initialization, we examine

the hourly accumulated precipitation for the first two hours of forecast and compare them with observations in both model and observational spaces. For the latter, the model predicted precipitation fields are interpolated to the sites of rain gauge stations. Availability of data limits our comparison to within SD though. Figures 8 and 9 show the precipitation comparisons for the 1st and 2nd hour, respectively.

Figure 8a shows the accumulated rainfall field from CNTL during the first hour and Fig. 8f the corresponding rainfall interpolated to stations. Compared to precipitation patterns of all other experiments and observations, the region of precipitation in this first hour of CNTL is much broader and the field appears smoother. The observed rainfall reaches 19 mm in the far north Shandong and has a secondary maximum of 9 mm in south-southwest Shandong (Figs. 8e,j), while the predicted values by CNTL at these locations are only 4 and 3 mm, respectively. Clearly, the rainfall is significantly under-predicted.

The rainfall prediction is improved significantly when cloud analysis is included and much more so when temperature adjustment is also invoked. Both CLDT and CLDTNCO predict two maximum precipitation centers along the shear line (Figs. 8c and 8d), with the maximum at the northern center being between 15 and 18 mm, close to the observed 19 mm. To the southwest of this overall maximum, along the Yellow River, both experiments predict maximum station values of 8 mm (Figs. 8h and 8i), which are very close to the observed values between 6 and 8 mm in this region (Fig. 8j). The corresponding values of CNTL are about 1 mm instead (Fig. 8f). Further south, the observed 9 mm rainfall (Fig. 8j) is under-predicted by both CLDT and CLDTNCO, with values around 4 mm (Figs. 8h and 8i).

The experiment with cloud analysis but without temperature adjustment, i.e., CLD (Fig. 8b and 8g), generally under-predicts the precipitation in this first hour everywhere. The

maximum values at the two centers along the shear line (also the Yellow River) are 9 and 6 mm, respectively, versus the observed 19 and 7 mm. This general under-prediction is more evident from the contour plot in Fig. 8b, indicating the importance of temperature adjustment associated with cloud analysis. This result is consistent with the findings of Hu et al (2005a), and is understandable because it is important to take into account of latent heat energy released into the system by prior precipitation.

Figure 9 shows the forecast and observed rainfall in the second hour. It is interesting to note that in this second hour, the difference in precipitation between CNTL and CLD has all but disappeared. Fig. 9a and Fig. 9b show almost identical pattern and amount and the station values in Fig. 9f and Fig. 9g are also very close. Both experiments, based on station values, under-predict, though, the precipitation associated with the overall maximum (11-12 mm versus observed 18 mm) as well as the rainfall to the southwest (1-3 mm versus observed 9 mm; compare Figs. 9f and 9g with Fig. 9j). We hypothesize here that adding cloud water and hydrometeors to the initial condition in CLD without adjusting temperature mainly helps improve the forecast of initial precipitation amount. After such added water rains out, the state of the atmosphere remains little affected, while further precipitation and the associated convection are mainly forced by the shear line and mesoscale vortex.

The situation is different with CLDT and CLDTNCO, which include temperature adjustment. The precipitation in the second hour is much heavier in these two cases compared to CNTL, with the maximum grid point values reaching 27 to 30 mm (Fig. 9c and Fig. 9d). As for the first hour, two centers are found along the shear line (and Yellow River), together with another strip of high precipitation that extends southwards. The latter is similar to the earlier two cases. The gridded analysis of observed rainfall suffers from the smoothing of the Cressman

objective analysis since the analyzed maximum of about 12 mm is much less than the observed 18 mm at a single station. This single-station maximum value is surrounded by stations with 13 mm or lower values though. Despite the seemingly over-prediction in terms of the maximum grid point values in CLDT and CLDTNCO (27 and 30 mm respectively), the maximum forecast values of 14 - 15 mm interpolated to the station locations match the observed maximum of 18 mm at one station and the 13 mm at the nearby stations reasonably well. If over-prediction indeed exists, it is more so with CLDTNCO, a tendency that is also revealed by the 6-h accumulated precipitation discussed earlier. It should also be noted that the rainfall in the north-south oriented strip in south SD is weakest in CLDT (Fig. 9c), whose interpolated station values in this region are closest to the observations (Fig. 9j). Therefore, CLDT is the better one among the best forecasts (CLDT and CLDTNCO). Clearly, the positive impact on QPF of full cloud analysis and of the 're-analysis' of conventional data is maintained into the second hour of prediction.

d. Bias and ETS scores

The bias scores (e.g., Anthes 1983) and equitable threat score (ETS, also called Gilbert skill score, Schaefer 1990) are used here to further assess the rainfall predictions. The scores are calculated based on around 100 surface stations in SD between observations and interpolated forecasts. The bias score $B = F/O$ is the ratio of the number of stations forecasted to reach or exceed a certain precipitation threshold (F) to the number of stations that actually exceed the threshold (O); a perfect forecast would have B=1, while values of B less than and greater than one represent under-predicting and over-predicting, respectively, the precipitation area coverage. The ETS score is defined as

$$\mathrm{T} = \frac{CF - CH}{F + O - CF - CH}, \text{ where } CH = \frac{F \cdot O}{N}.$$

CF is the number of correctly forecast stations (both model and observations produce precipitation at or above a given threshold), F and O are as defined above, N is the number of points within the verification area. The ETS score can evaluate the position accuracy of a forecast. Because most of the hourly observations in SD are no more than 15 mm during the 6 hours, we choose to calculate the scores for 2.5 mm, 5 mm and 10 mm thresholds.

The left column of Fig. 10 presents the hourly precipitation bias scores of the four experiments for 2.5 mm, 5 mm and 10 mm thresholds from 1 to 6 hours, and the right column contains the corresponding ETS scores. As shown in the figure, there is a significant low bias with CNTL (solid) within the first hour of forecast, obviously due to the spin-up required of this non-cloud-analysis run. The bias errors with CLD are much smaller at hour 1; in fact, they are the smallest among all four experiments at this time. The ETS score of CLD is also the highest for the 2.5 mm and 5 mm thresholds in the first hour. Apparently, adding water to the system without corresponding temperature perturbations allows the water to rainout quickly, resulting in a smallest low bias of precipitation in the first hour for light rain. After hour 2, the bias and ETS scores of CNTL (solid) and CLD (long dashed) are very similar and generally show low biases for the first two thresholds. For the 10 mm threshold, the scores of CNTL and CLD are nearly the same (the two curves overlap for the first 5 hours in Fig. 10e and for the first 3 hours in Fig. 10f), and the bias errors are larger than the other two cases. Basically, the effect of cloud analysis is lost beyond the first hour in CLD, consistent with our earlier discussions. Furthermore, as shown in Figs. 10e and 10f, heavy rainfall forecast is not improved without temperature adjustment.

The scores for CLDT and CLDTNCO are very good. The bias scores are close to 1 after the first hour, and are well maintained for most of the 6-hour period. The ETS scores for CLDT

and CLDTNCO are higher than the other two cases in at least the first 3 hours for all thresholds. The scores near the end of period become close to each other, for all experiments except the bias scores at the 5 mm thresholds, where CLDT and CLTTCNO continue to outperform the other two runs.

It is found that the ETS scores of CLDT are worse than those of CLDTNCO in the first two hours but become generally better afterwards. The initially better ETS scores and smaller low-bias errors in CLDTNCO appear to be related to the difference in the initial fields near 37.07°N, 114.50°E, where a cold center at 850hPa was observed by sounding No. 53798, which was not re-analyzed on the ARPS grid in CLDTNCO. The absence of this cold center helped increase the initial precipitation and improve the precipitation scores. This behavior should probably be regarded as a coincidence rather than a general indication of negative impact by sounding data. The lower scores of CLDTNCO compared to CLDT starting from the third hour suggests that overall the analysis of conventional data is still beneficial. This is also supported by our earlier observation that the 6-h total precipitation is better predicted by CLDT than by CLDTNCO.

Figure 11 shows the bias and ETS scores of the accumulated rainfall over entire 6 hours, for different thresholds and experiments. It can be seen from Fig. 11a that the bias scores for the lowest 10 mm threshold are close to 1 for all three experiments with cloud analysis, with CNTL slightly under-predicting the amount. Therefore, light precipitation over the entire 6 hour period is handled well by the model with and without cloud analysis, although we know from earlier discussions that during the first a couple of hours CNTL probably still significantly under-predicts even the low threshold values.

For most other thresholds, both bias and ETS scores are clustered into two groups, one

containing CNTL and CLD and the other containing CLDT and CLDTNCO (Fig. 11). The scores of the second group are clearly better than those of the first group. For example, the ETS scores for thresholds 60 and 70 mm are zero for CNTL and CLD in the first group but over 0.35 for the runs in the second group while the bias scores tell a similar story. Considering the fact that the maximum observed 6-h precipitation is 79 mm and only three stations have precipitation over 70 mm, the reasonable scores for 70 mm threshold indicate that experiments CLDT and CLDTNCO did a very good job at capturing localized heavy precipitation. The other two experiments basically failed to predict such heavy precipitation, giving zero scores at the high thresholds.

d. Time evolution of cloud-scale perturbations

To better understand how the model responds to the initial perturbations introduced by the initial analysis, and to see how the cloud-scale perturbations evolve with time, we calculate and plot the mean values of q_c, w and θ' in an area within 36-38°N, 116-118°E at the 4 km height. As can be seen from Fig. 12a, the mean q_c has relatively high values (> 0.7 g kg^{-1}) at the initial time for the three experiments (CLD, CLDT and CLDTNCO) that include cloud analysis with the value exceeding, but decreases quickly to below 0.3 g kg^{-1} in the first hour, apparently due to microphysical convection and rainout. In contrast, the mean value of q_c in CNTL is much lower in the initial field (<0.1 g kg^{-1}) but increases quickly within the first hour to approach the values of the other three. The mean q_c values with temperature adjustment remain higher than the cases of CNTL and CLD until about 5.5 hours.

From Fig. 12b, it is seen that the initial values of w in CNTL, CLD and CLDT are essentially the same (~0.1 m s^{-1}) while that of CLDTNCO is slightly higher (0.12 m s^{-1}). The mean w of CLDT and CLDTNCO increases quickly in the first hour to above 0.18 m s^{-1}, obviously due to added buoyancy, an remains at higher values for the next 5 hours. On the

contrary, it takes CNTL and CLD a long time to spin up the *w*, although after being spun-up, it eventually overtakes those of CLDT and CLDTNCO, the latter happens because of the presence of mesoscale forcing and the eventual release of the convective energy. We also note that the more significant increase in *w* in CNTL and CLD after hour 3 happens after the temperature perturbation reaches the level of the cases with initial temperature adjustment (Fig. 12c). The mean θ' of CLDT and CLDTNCO decreases quickly in the first hour from the initially high values, suggesting that a significant amount of adjustment was happening in the model, but the value levels off after the first hour.

It is clear therefore that the changes in the cloud-scale perturbations depends mostly on whether temperature adjustment is performed in the cloud analysis, and this adjustment is critical for the promotion and maintenance of convection and for the mitigation of model "spin-up" problem. The impact of the complex cloud analysis is most significant on the convection intensity in the first 3-4 hours and is maintained beyond 5 hours.

5. Comparison of model-predicted precipitation with radar-estimated rainfall

We compare the model precipitation in the first hour of forecast with radar estimated rainfall. The radar rainfall estimation uses the standard semi-empirical reflectivity-rain-rate ($Z-R$) relationship $Z=300R^{1.4}$ (Woodley et al. 1975; Doviak and Zrnic 1993) and accumulates the rainfall over the one hour period, using radar data at 6 min time intervals. Studies have found that the hourly precipitation accumulation estimates in the 40 to 150 km range of radar in spring and summer and 40 to 100 km range of radar in winter and fall are useful in heavy rain events although there is a systematic underestimation (Smith et al. 1996) and the estimate may suffer from bright-band effects (Baeck and Smith 1998). Here we compare the model precipitation in the first hour of forecast with radar hourly precipitation accumulation

estimates.

Figure 13 shows the radar hourly precipitation accumulation estimates ending at 01 UTC 11 October 2003. It can be seen that the distribution of the estimated rainfall is similar to the rain gauge observations, but the maximum amount within 40 to 100 km is only 2.5 mm, a severe under-estimation of the observed maximum of 19 mm (c.f., Fig. 8j). In contract, the forecasts of CLDT, CLDTNCO or even CLD are much better. These results suggest that a mesoscale model properly initialized using radar reflectivity data has the potential to predict precipitation amount, even in the short term, better than the precipitation estimation using standard Z-*R* relationship. We do realize that more sophisticated rainfall estimation algorithms, that include rain gauge calibration, may be able to do a better job. They are, however, rainfall estimation rather than forecast in any case.

6. Conclusions

For the quantitative forecast of heavy rainfall that developed along a shear line with an embedded mesoscale vortex in North China, the impacts of a three-dimensional complex cloud analysis scheme using radar reflectivity data from a Chinese operational Doppler radar are investigated. Comparisons between forecast rainfall from cases with and without cloud analysis and with and without cloud-scale temperature adjustment are made with the following conclusions:

1) The changes in the cloud-scale perturbations are found to depend mostly on whether temperature adjustment is performed in the cloud analysis, and this adjustment is critical for the promotion and maintenance of convection and for the mitigation of model “spin-up” problem. The impact of the complex cloud analysis is most significant on the convection intensity in the first 3-4 hours and is maintained beyond 5 hours.

2) When the cloud analysis is performed without the temperature adjustment due to latent heat release, the impact on the overall system lasts for only one hour. The improvement to the precipitation forecast is confined to light rain only for the lack of temperature adjustment. The initial precipitation amount is improved, mainly due to the fallout of the added water. Because of strong mesoscale forcing associated with this precipitation system, precipitation does develop eventually, but there is a delay of several hours and the total precipitation in the first 6 hours is under-predicted significantly.

3) When temperature adjustment in the ADAS cloud analysis procedure is activated, both the spatial distribution and amount of forecast precipitation are improved. In fact, the predicted precipitation maxima are very close to the observed values. The temporal distribution of precipitation is also very good.

4) The 're-analysis' of convectional surface and upper-air observations on the native 6-km ARPS grid data is found to also beneficial, though the impact is much smaller than cloud analysis.

5) When properly initialized via the complex analysis, the model predicted precipitation is found to be more accurate than the radar hourly precipitation accumulation estimates based on a standard semi-empirical Z-*R* relationship, even in the first hour when typical forecasts suffer from the spinup problem.

Acknowledgements. The authors thank Ming Hu of the University of Oklahoma for helpful discussions. The work was mainly supported by the Key Project of National Natural Science Foundation of China (Grant No. 40433007), the Olympic Project (Grant No. KACX1-02), and the “Outstanding Oversea Scholars” Award of Chinese Academy of Sciences to Ming Xue (Grant No. 2004-2-7). Ming Xue was also supported by NSF grants ATM-0129892, ATM-0331594,

ATM-0331756 and EEC-0313747, and DOT-FAA grant NA17RJ1227.

References

Anthes RA (1983) Regional Models of the Atmosphere in Middle Latitudes. Mon Wea Rev 111: 1306-1335

Aonashi K (1993) An initialization method to incorporate precipitation data into a mesoscale numerical weather prediction model. J Meteor Soc 71: 393-406

Baeck ML, Smith JA (1998) Rainfall Estimation by the WSR-88D for Heavy Rainfall Events. Wea Forecasting 13: 416-436

Bratseth AM (1986) Statistical interpolation by means of successive corrections. Tellus 38A: 439-447

Brewster K (1996) Application of a Bratseth analysis scheme including Doppler radar data. Preprints, 15th Conf Wea Anal Forecasting. Norfolk: VA, Amer Meteor Soc, 92-95

Brewster K (2002) Recent advances in the diabatic initialization of a non-hydrostatic numerical model. Preprints, 15th Conf Num Wea Pred. San Antonio: TX, Amer Meteor Soc, J6.3

Davolio S, Buzzi A (2004) A nudging scheme for the assimilation of precipitation data into a mesoscale model. Wea Forecasting 19: 855-871

Dawson DTII, Xue M (2005) Numerical forecasts of the 15-16 June 2002 Southern Plains severe MCS: Impact of mesoscale data and cloud analysis. Mon Wea Rev. Conditionally accepted

Doviak R, Zrnic D (1993) Doppler Radar and Weather Observations. 2nd Ed Academic Press, 562 pp

Falkovich A, Kalnay E, Lord S, Muthur MB (2000) A new method of observed rainfall assimilation in forecast models. J Appl Meteor 39: 1282-1298

Gao J-D, Xue M, Brewster K, Droegemeier KK (2004) A three-dimensional variational data analysis method with recursive filter for Doppler radars. J Atmos Oceanic Tech 21: 457-469

Hu M, Xue M, Gao J-D, Brewster K (2005a) 3DVAR and cloud analysis with WSR-88D Level-II data for the prediction of Fort Worth tornadic thunderstorms. Part I: Impact of radial velocity analysis via 3DVAR. Mon Wea Rev. Accepted

——, ——, and Brewster K (2005b) 3DVAR and cloud analysis with WSR-88D Level-II data for the prediction of Fort Worth tornadic thunderstorms. Part II: Cloud analysis and its impact. Mon Wea Rev. Accepted

Kasahara A, Balgovind RC, Katz B (1988) Use of satellite radiometric imagery data for improvement in the analysis of divergent wind in the tropics. Mon Wea Rev 116: 866–883

Krishnamurti TN, Bedi HS, Ingles K (1993) Physical initialization using SSM/I rain rates. Tellus 45A: 247-269

Lee M-S, Lee D-K (2003) An application of a weakly constrained 4DVAR to satellite data assimilation and heavy rainfall simulation. Mon Wea Rev 131: 2151-2176

Lin Y-L, Farley RD, Orville HD (1983) Bulk parameterization of the snow field in a cloud model. J Climate Appl Meteor 22: 1065-1092

Manobianco J, Koch S, Karyampudi VM, Negri AJ (1994) The impact of assimilating satellite-derived precipitation rates on numerical simulations of the ERICA IOP 4 cyclone. Mon Wea Rev 122: 341-365

Puri K, Miller MJ (1990) The use of satellite data in the specification of convective heating for diabatic initialization and moisture adjustment in numerical weather prediction models. Mon Wea Rev 118: 67-93

Puri K, Davidson NE (1992) The use of infrared satellite cloud imagery data as proxy data for moisture and diabatic heating in data assimilation. Mon Wea Rev 120: 2329-2341

Rogers RF, Fritsch JM, Lambert WC (2000) A simple technique for using radar data in the

dynamic initialization of a mesoscale model. Mon Wea Rev 128: 2560-2574

Schaefer JT (1990) The critical success index as an indicator of warning skill. Wea Forecasting 5: 570-575

Smith PL, Jr, Myers CG, Orville HD (1975) Radar reflectivity factor calculations in numerical cloud models using bulk parameterization of precipitation processes. J Appl Meteor 14: 1156-1165

Smith JA, Seo DJ, Baeck ML, Hudlow MD (1996) An intercomparison study of NEXRAD precipitation estimates. Water Resource Research 32: 2035-2045

Souto MJ, Balseiro C, Pérez-Muñuzuri FV, Xue M, Brewster K (2003) Impact of Cloud Analysis on Numerical Weather Prediction in the Galician Region of Spain. J Appl Meteor 42: 129-140

Takano I, Segami A (1993) Assimilation and initialization of a mesoscale model for improved spin-up of precipitation. J Meteor Soc Japan 71: 377-391

Wang W, Warner TT (1988) Use of four-dimensional data assimilation by Newtonian relaxation and latent-heat forcing to improve a mesoscale-model precipitation forecast: A case study. Mon Wea Rev 116: 2594-2613

Weng F, Liu Q (2003) Satellite data assimilation in numerical weather prediction models. Part I: Forward radiative transfer and Jacobian modeling in cloudy atmospheres. J Atmos Sci 60: 2633-2646

Woodley WL, Olsen AR, Herndon A, Wiggert V (1975) Comparison of gage and radar methods of convective rain measurement. J Appl Meteor 14: 909-928

Wu X, Diak GR, Hayden CM, Young JA (1995) Short-range precipitation forecasts using assimilation of simulated satellite water vapor profiles and column cloud liquid water amounts. Mon Wea Rev 123: 347-365

Xue M, Droegemeier KK, Wong V, Shapiro A, Brewster K (1995) ARPS Version 4.0 User's Guide. Center for Analysis and Prediction of Storms, University of Oklahoma, 380pp

——, ——, and —— (2000) The Advanced Regional Prediction System (ARPS) – A multi-scale nonhydrostatic atmospheric simulation and prediction model. Part I: Model dynamics and verification. Meteor Atmos Phys 75: 161-193

——, ——, ——, ——, ——, Carr F, Weber D, Liu Y, Wang D-H (2001) The Advanced Regional Prediction System (ARPS) – A multi-scale nonhydrostatic atmospheric simulation and prediction model. Part II: Model physics and applications. Meteor Atmos Phys 76: 143-165

——, Wang D-H, Gao J-D, Brewster K, Droegemeier KK (2003) The advanced regional prediction system (ARPS), storm-scale numerical weather prediction and data assimilation. Meteor Atmos Phys 82: 139-170

Yucel I, Shuttleworth WJ, Gao X, Sorooshian S (2003) Short-term performance of MM5 with cloud-cover assimilation from satellite observations. Mon Wea Rev 131: 1797–1810

Zhang J, Carr F, Brewster K (1998) ADAS cloud analysis. Preprints, 12th Conf Num Wea Pred. Phoenix: AZ, Amer Meteor Soc, 185-188

—— (1999) Moisture and Diabatic Initialization based on Radar and Satellite Observations. Ph. D. Dissertation. University of Oklahoma, 194 pp

Zhu X-Y, Zhu J-J (2004) New Generation Weather Radar in China. Chinese Meteorological Science and Technology 32: 255-258 (in Chinese)

List of Table

Table 1. List of 6 km experiments

Experiment name	Cloud analysis	Temperature adjustment	Conventional data
CNTL	No	No	Yes
CLD	Yes	No	Yes
CLDT	Yes	Yes	Yes
CLDTNCO	Yes	Yes	No

Figure captions

Fig. 1. Surface station plots and mean sea level pressure (a), and 850 hPa geopotential height and station plots (b), at 00 UTC or 08 LST, 11 October 2003. The sky was mostly cloudy for the domain in (a). The shear line along an inverted trough is in dark bold in (b), and 'L' indicates the center of mesoscale vortex.

Fig. 2. Qihe Doppler radar composite reflectivity at 00 UTC or 08 LST, 11 October 2003.

Fig. 3. Computational domains for the 30 km and 6 km resolution grids. The black dot indicates the location of Qihe radar. Yangtze (Changjiang) River and Yellow (Huanghe) River are drawn in the figure as thick black lines. Within the 6 km domain, Yellow River passes by the radar site. In the figure, SD refers to Shandong province, AH to Anhui province, JS to Jiangsu province, HN to Henan province and HB to Hebei province.

Fig. 4. Wind field and pressure field at 850hPa height at 06 UTC 11 Oct. 2003 from (a) the 30 km grid forecast and (b) NCEP analysis. Shear line is in dark bold, and 'L' indicates the center of mesoscale vortex.

Fig. 5. The vertical cross-section of the analysis increments of (a) q_c, (b) q_r, (c) q_i, and (d) q_s ($\times 10^{-1}$, g kg^{-1}), and (e) potential temperature, θ (K), along 37°N with ADAS cloud analysis.

Fig. 6. The vertical cross-section of radar reflectivity (dBZ) along 37°N at 00 UTC 11 Oct. 2003.

Fig. 7. Forecast 6-h accumulated rainfall (mm) from 6-km experiments, (a) CNTL, (b) CLD, (c) CLDT, (d) CLDTNCO, and (e) the corresponding rain gauge observed rainfall.

Fig. 8. Upper panel: accumulated precipitation for the hour ending at 01 UTC, from (a) CNTL,

(b) CLD, (c) CLDT, (d) CLDTNCO, and (e) for rain gauge observations. Lower panel: the corresponding forecast precipitation interpolated the rain gauge stations, as compared to the rain gauge observations. Hourly precipitation data were not available to the authors outside Shandong Province.

Fig. 9. As Fig. 8, but for the accumulated precipitation in the second hour, ending at 02 UTC, October 11, 2003.

Fig. 10. Bias scores (left column) and ETS (right column) of hourly precipitation for experiments CNTL (solid lines), CLD (long dashed lines), CLDT (long-short dashed lines) and CLDTNCO (dot-dot-dashed lines), for 2.5 mm (upper panel), 5 mm (middle panel), and 10 mm (lower panel) thresholds.

Fig. 11. Bias scores (a), and ETS scores (b), for 6-h accumulated rainfall for experiments CNTL (solid lines), CLD (long dashed lines), CLDT (long-short dashed lines) and CLDTNCO (dot-dot-dashed lines), plotted for different thresholds.

Fig. 12. The time series of mean q_c (a), w (b), and θ' (c), in the region between 36-38°N and 116-118°E at 4 km height, for CNTL (solid), CLD (long dashed), CLDT (long short dashed) and CLDTNCO (dot-dot-dashed lines).

Fig. 13. Radar-based hourly precipitation accumulation estimate at 01 UTC 11 October 2003.

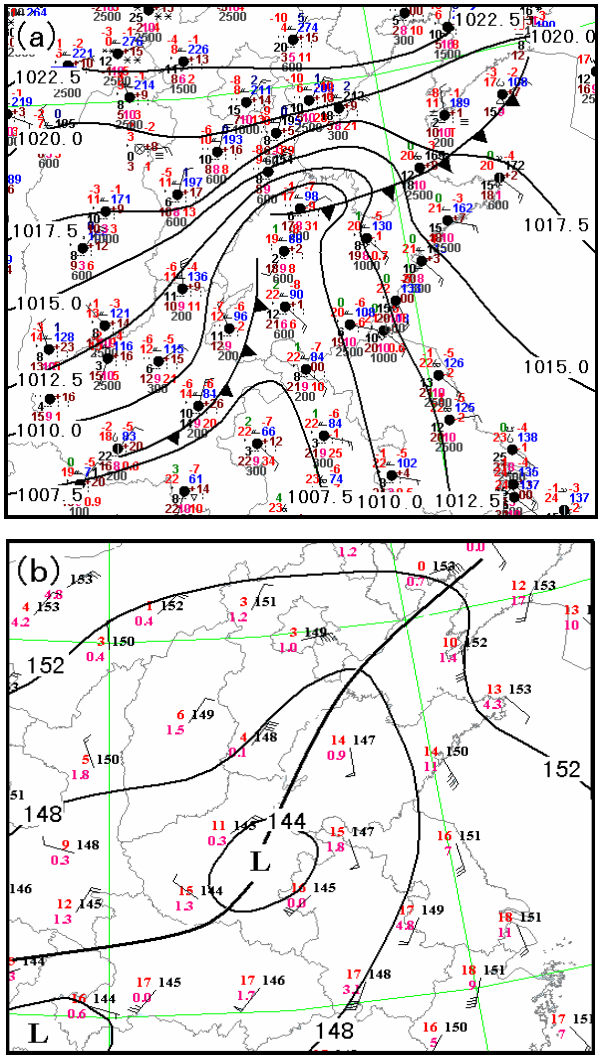

Fig. 1. Surface station plots and mean sea level pressure (a), and 850 hPa geopotential height and station plots (b), at 00 UTC or 08 LST, 11 October 2003. The sky was mostly cloudy for the domain in (a). The shear line along an inverted trough is in dark bold in (b), and 'L' indicates the center of mesoscale vortex.

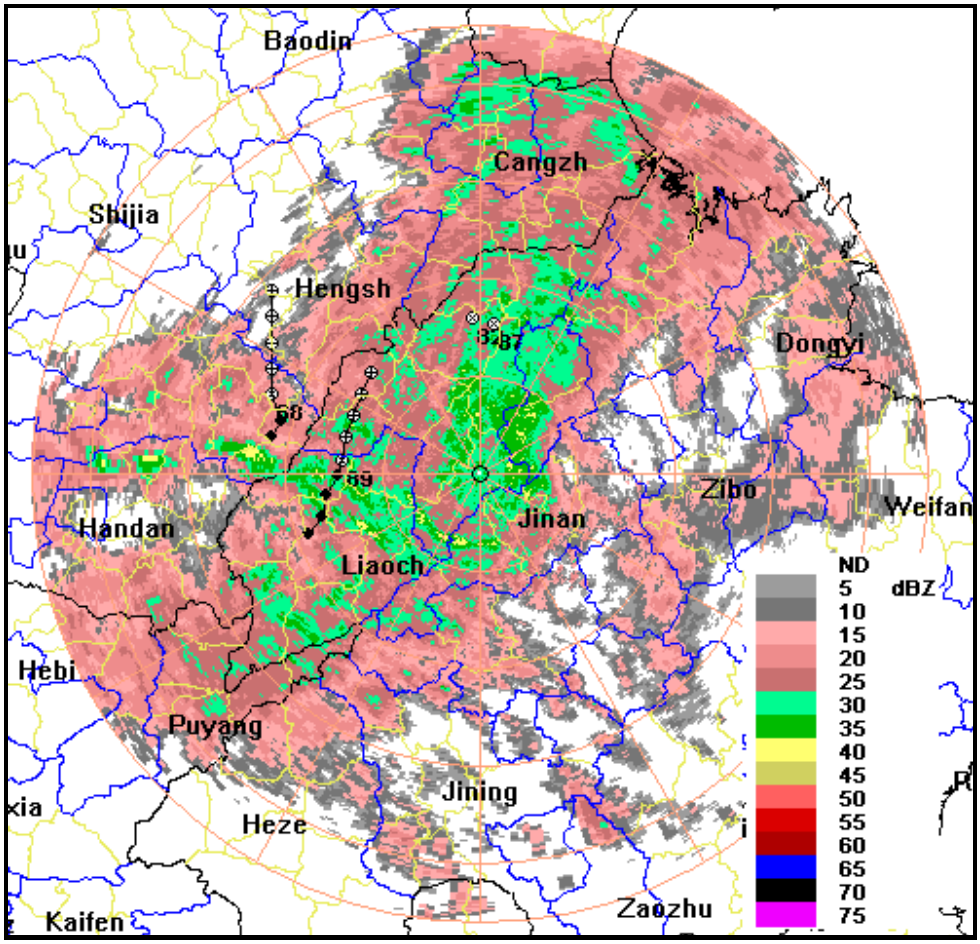

Fig. 2. Qihe Doppler radar composite reflectivity
at 00 UTC or 08 LST, 11 October 2003.

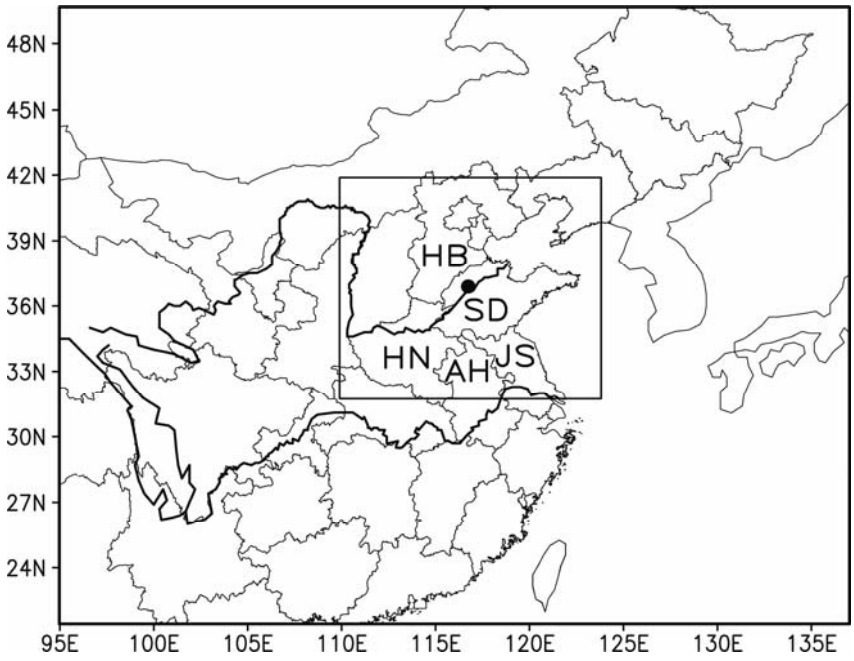

Fig. 3. Computational domains for the 30 km and 6 km resolution grids. The black dot indicates the location of Qihe radar. Yangtze (Changjiang) River and Yellow (Huanghe) River are drawn in the figure as thick black lines. Within the 6 km domain, Yellow River passes by the radar site. In the figure, SD refers to Shandong province, AH to Anhui province, JS to Jiangsu province, HN to Henan province and HB to Hebei province.

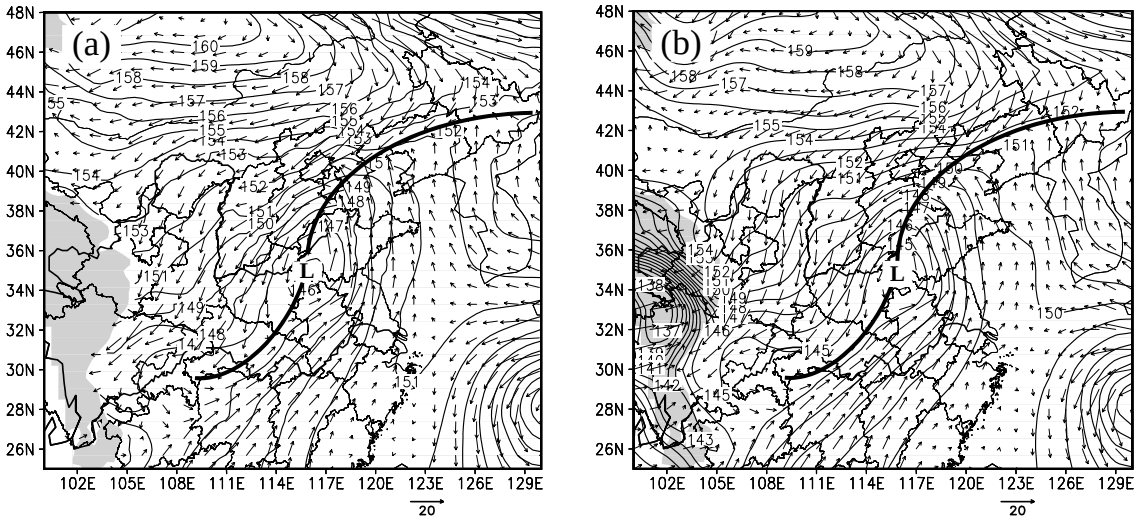

Fig. 4. Wind field and pressure field at 850hPa height at 06 UTC 11 Oct. 2003 from (a) the 30 km grid forecast and (b) NCEP analysis. Shear line is in dark bold, and 'L' indicates the center of mesoscale vortex.

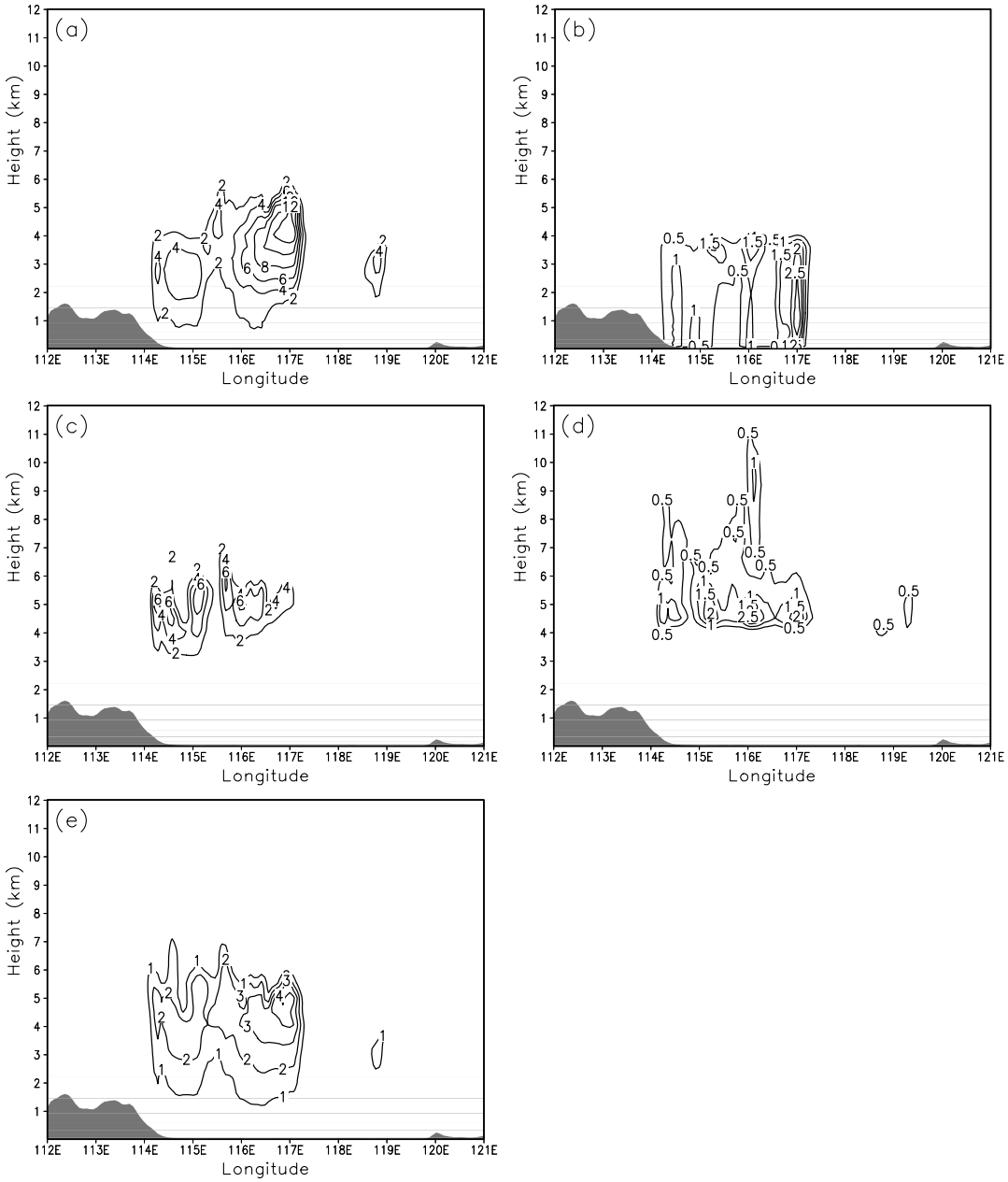

Fig. 5. The vertical cross-section of the analysis increments of (a) q_c, (b) q_r, (c) q_i, and (d) q_s ($\times 10^{-1}$, g kg^{-1}), and (e) potential temperature, θ (K), along 37°N with ADAS cloud analysis.

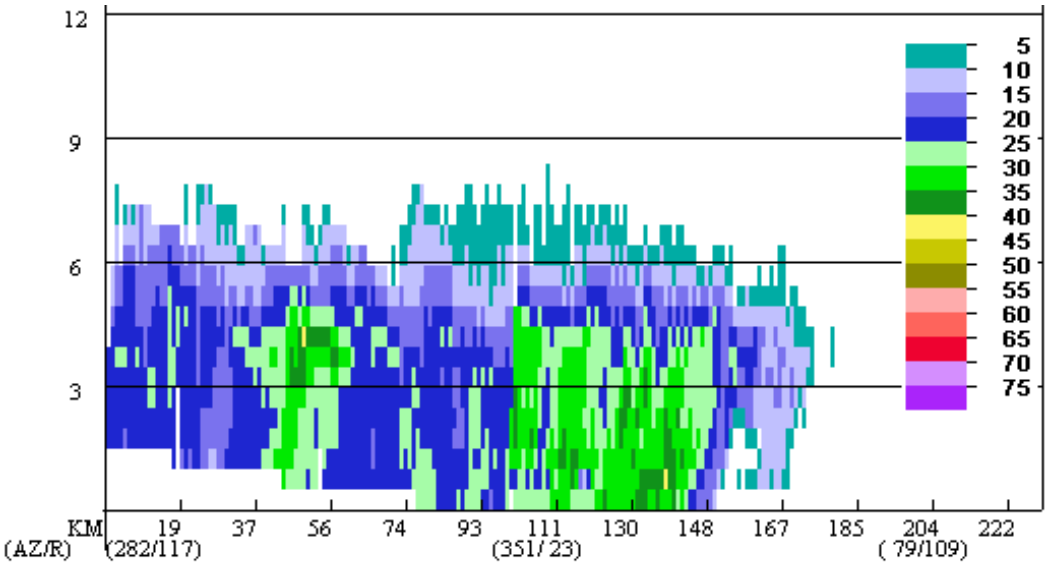

Fig. 6. The vertical cross-section of radar reflectivity (dBZ) along 37°N at 00 UTC 11 Oct. 2003.

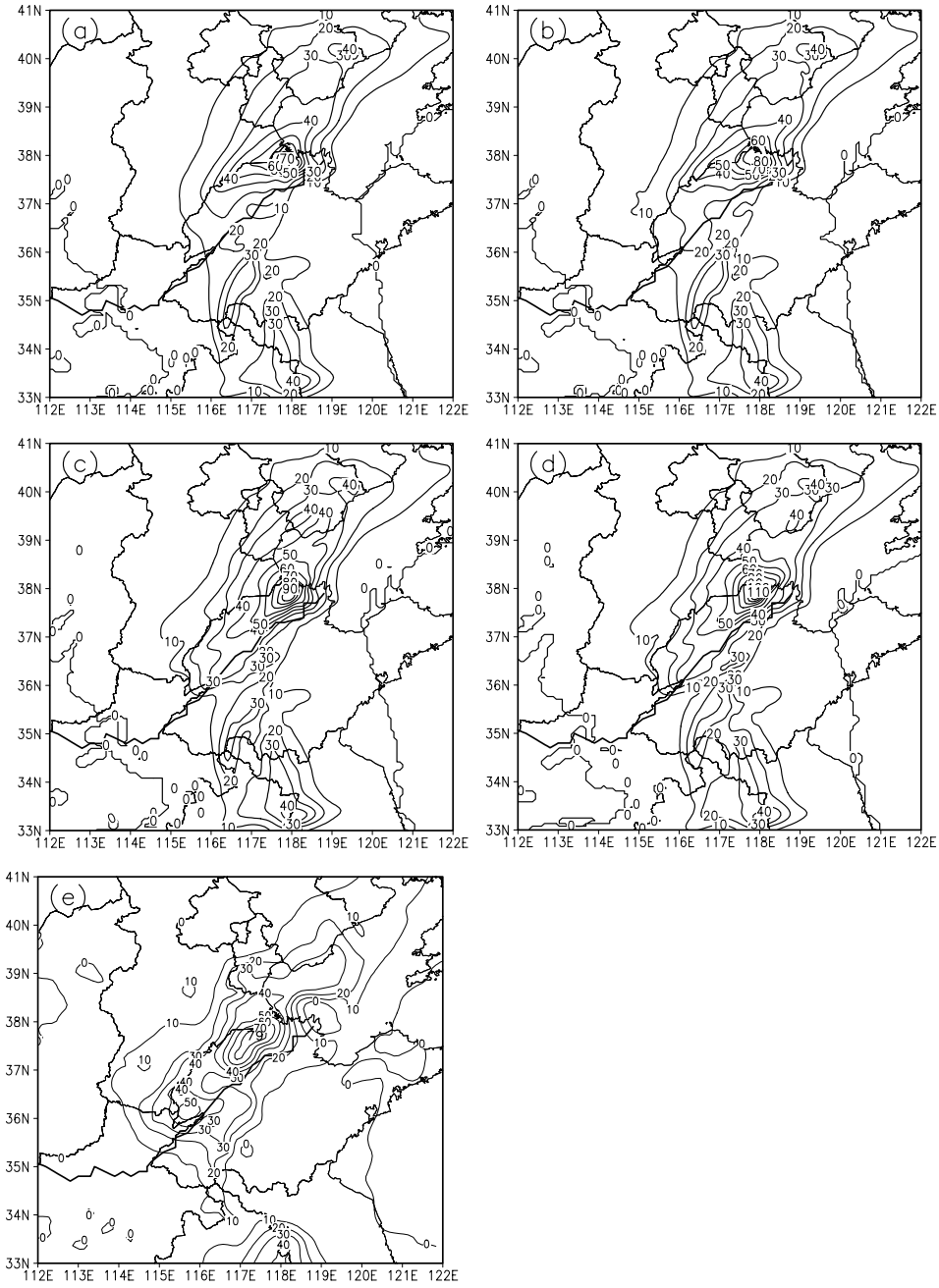

Fig. 7. Forecast 6-h accumulated rainfall (mm) from 6-km experiments, (a) CNTL, (b) CLD, (c) CLDT, (d) CLDTNCO, and (e) the corresponding rain gauge observed rainfall.

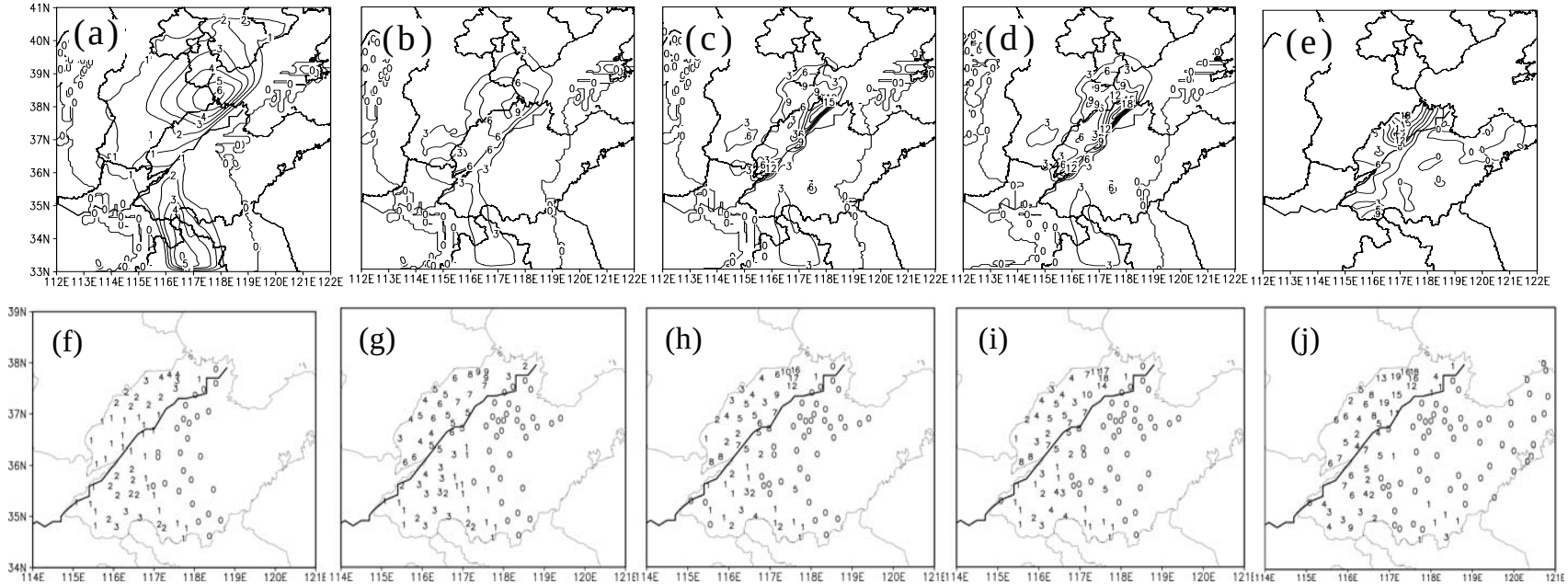

Fig. 8. Upper panel: accumulated precipitation for the hour ending at 01 UTC, from (a) CNTL, (b) CLD, (c) CLDT, (d) CLDTNCO, and (e) for rain gauge observations. Lower panel: the corresponding forecast precipitation interpolated the rain gauge stations, as compared to the rain gauge observations. Hourly precipitation data were not available to the authors outside Shandong Province.

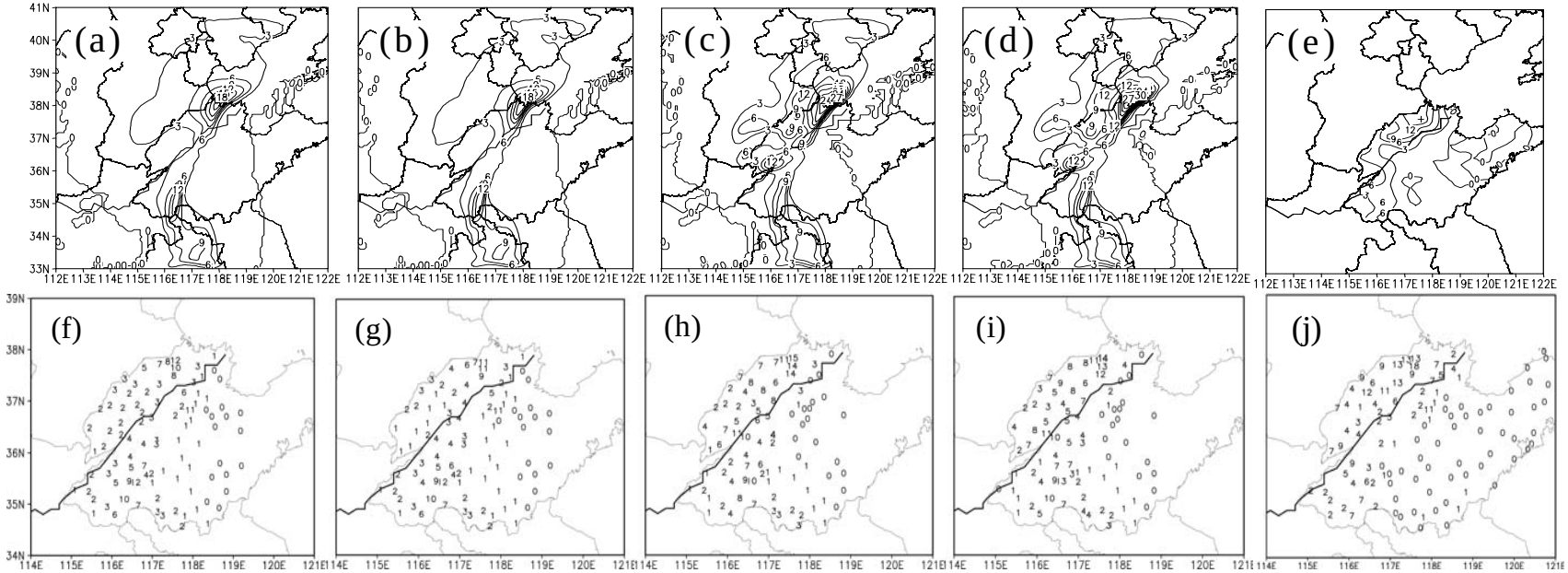

Fig. 9. As Fig. 8, but for the accumulated precipitation in the second hour, ending at 02 UTC, October 11, 2003.

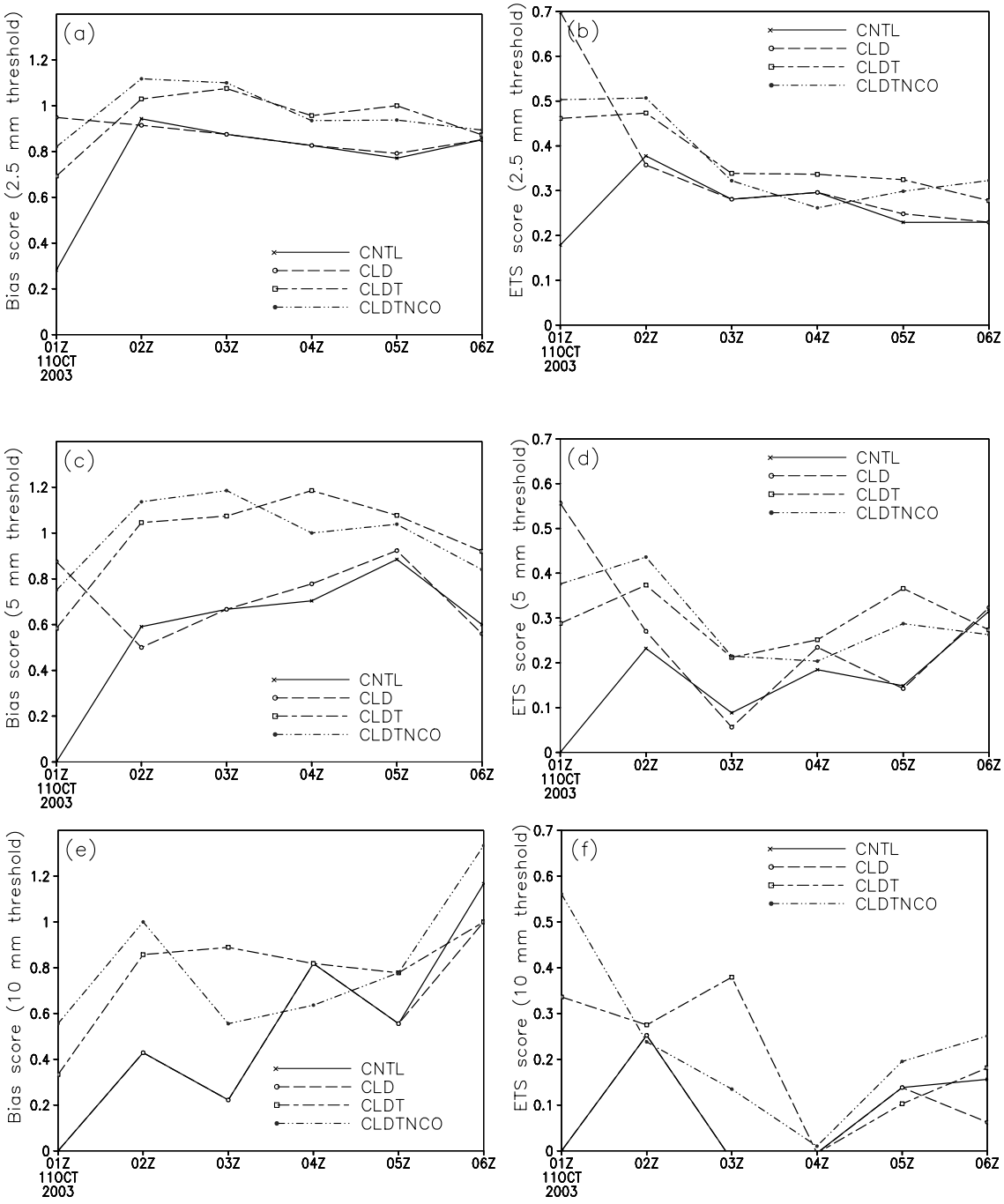

Fig. 10. Bias scores (left column) and ETS (right column) of hourly precipitation for experiments CNTL (solid lines), CLD (long dashed lines), CLDT (long-short dashed lines) and CLDTNCO (dot-dot-dashed lines), for 2.5 mm (upper panel), 5 mm (middle panel), and 10 mm (lower panel) thresholds.

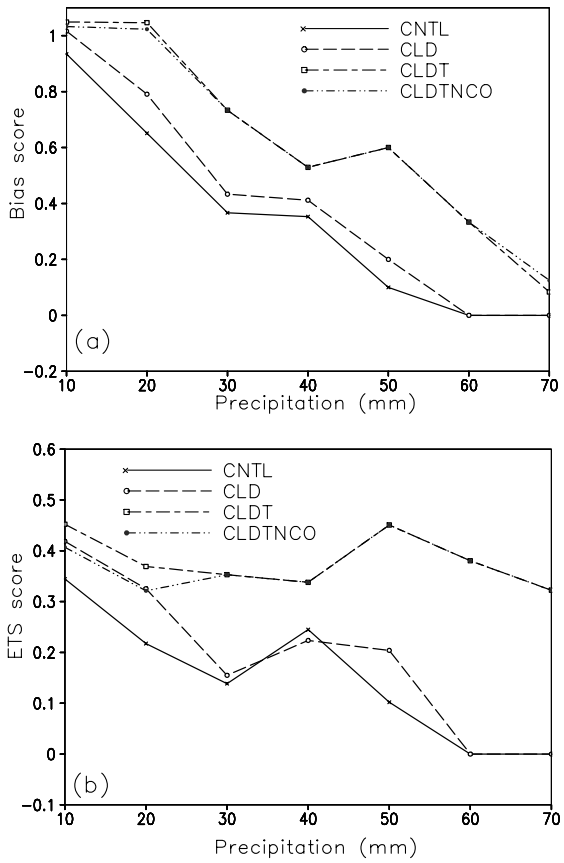

Fig. 11. Bias scores (a), and ETS scores (b), for 6-h accumulated rainfall for experiments CNTL (solid lines), CLD (long dashed lines), CLDT (long-short dashed lines) and CLDTNCO (dot-dot-dashed lines), plotted for different thresholds.

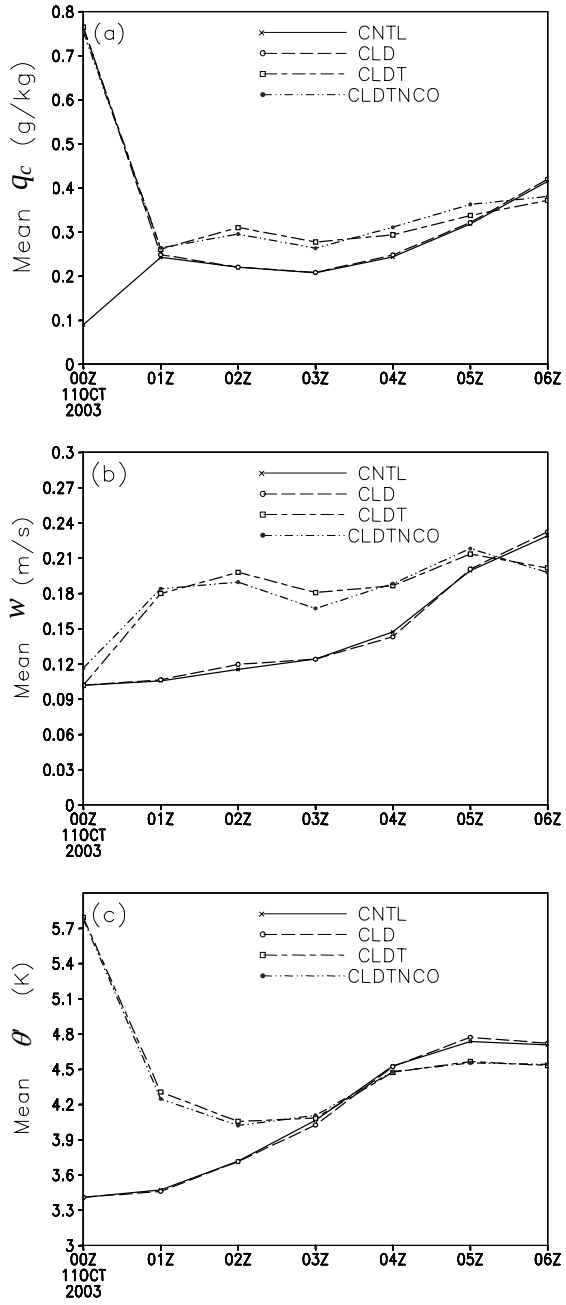

Fig. 12. The time series of mean q_c (a), w (b), and θ' (c), in the region between 36-38°N and 116-118°E at 4 km height, for CNTL (solid), CLD (long dashed), CLDT (long short dashed) and CLDTNCO (dot-dot-dashed lines).

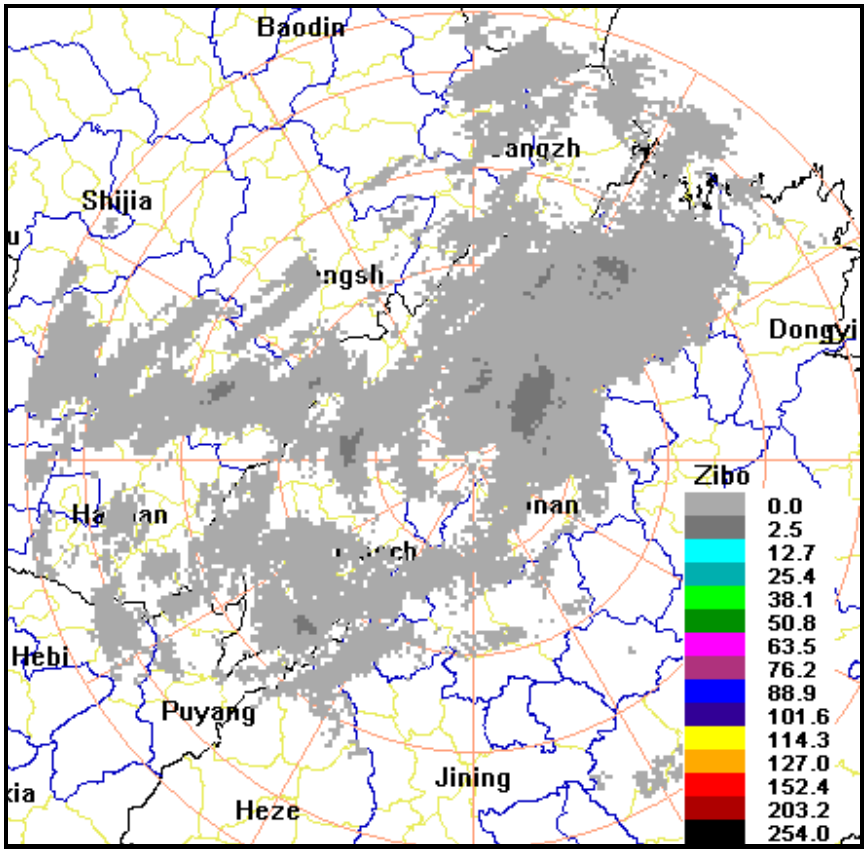

Fig. 13. Radar-based hourly precipitation accumulation estimate at 01 UTC 11 October 2003.